GW calculations using the spectral decomposition of the dielectric matrix: Verification, validation, and comparison of methods

T. Anh Pham, Huy-Viet Nguyen, Dario Rocca, and Giulia Galli

Phys. Rev. B **87**, 155148 — Published 26 April 2013

DOI: 10.1103/PhysRevB.87.155148

GW calculations using the spectral decomposition of the dielectric matrix: verification, validation and comparison of methods

T. Anh Pham,[1,2,*] Huy-Viet Nguyen,[3,†] Dario Rocca,[1,‡] and Giulia Galli[1,4]

[1] *Department of Chemistry, University of California, Davis, California, 95616, USA*
[2] *Lawrence Livermore National Laboratory, Livermore, California, 94551, USA*
[3] *Institute of Physics, Vietnam Academy of Science and Technology, 18 Hoang Quoc Viet, Cau Giay, Hanoi, Vietnam*
[4] *Department of Physics, University of California, Davis, California, 95616, USA*

(Dated: April 3, 2013)

In a recent paper [Phys. Rev. B 85, 081101(R) (2012)] we presented an approach to evaluate quasiparticle energies based on the spectral decomposition of the static dielectric matrix. This method does not require the calculation of unoccupied electronic states, nor the direct diagonalization of large dielectric matrices, and it avoids the use of plasmon-pole models. The numerical accuracy of the approach is controlled by a single parameter, i.e., the number of eigenvectors used in the spectral decomposition of the dielectric matrix. Here we present a comprehensive validation of the method, encompassing calculations of ionization potentials and electron affinities of various molecules and of band gaps for several crystalline and disordered semiconductors. We demonstrate the efficiency of our approach by carrying out GW calculations for systems with several hundreds of valence electrons.

PACS numbers: 71.15.Qe, 31.15.xm, 71.15.Mb

I. INTRODUCTION

Calculations based on density functional theory[1] (DFT) are widely used in condensed matter physics and chemistry to study the structural and electronic properties of molecules, nanostructures and materials. However, in principle DFT calculations with approximate exchange correlation functionals are limited to ground state properties; often, when used to describe electronic excitation processes, these calculations do not yield good, quantitative agreement with experiments, although they may account for trends in specific properties within given classes of materials or molecules.[2]

A formal basis for studying electronic excitation processes in materials is provided by many-body perturbation theory (MBPT).[3,4] In particular, in the mid-60s an approach was introduced by Hedin, to describe the direct and inverse photoemission spectra of solids and to compute ionization potentials and electron affinities of molecules, the so called GW approach.[5] It then took two decades to develop efficient techniques to apply such a method to solids, e.g., crystalline semiconductors. Since the pioneering work of Hybertsen and Louie,[6] the GW approximation to quasiparticle energies has been widely used to study fundamental band gaps,[7] band offsets at interfaces,[8] and quantum transport in molecular contacts.[9] In addition, quasiparticle energies obtained within the GW approximation may be used as input for the solution of the Bethe-Salpeter equation, an alternative method to time-dependent density functional theory for the calculation of absorption spectra.[4]

Despite its success over the past two and a half decades, the use of the GW approximation to study materials and molecules still faces several numerical challenges. One of the difficulties in computing quasiparticle energies is the evaluation of the dielectric matrix (ϵ) used to describe the electronic polarization and screening of a system subjected to an external electromagnetic perturbation. Several approximations have been developed to reduce the computational workload required to evaluate ϵ, including the use of plasmon-pole models to approximate the frequency dependence of ϵ, and the use of modest plane-wave cutoffs to represent the dielectric matrix with a plane-wave basis set.[6] Furthermore, the direct evaluation of both the Green's function (G) and the dielectric matrix entering the expression of the screened Coulomb interaction (W) requires summations over an infinite number of unoccupied electronic states. In practice, such summations are truncated at a finite number of unoccupied states, and the convergence of the computed quasiparticle energies as a function of this number needs to be carefully checked for each specific system.[10–13]

Recently, we developed a technique[14] for the evaluation of quasiparticle energies aimed at improving both the computational efficiency and the control of numerical errors of existing methodologies. Our approach does not require the calculation of unoccupied electronic states, nor the direct diagonalization of large dielectric matrices, and it avoids the use of plasmon pole models. Most importantly, its numerical accuracy is controlled by a single parameter, i.e. the number of eigenvalues and eigenvectors used in the spectral decomposition of the static dielectric matrix. In the last few years, several other techniques have appeared in the literature, which overcome or alleviate the problem of summing over large numbers of unoccupied states.[12,15–17]

In this paper we discuss in detail the accuracy and efficiency of the approach we first introduced in Ref. 14. We compare results for ionization potentials, electron affinities and band structures with those of existing GW cal-

culations, and we address the convergence of quasiparticle energies with respect to the number of unoccupied states, as well as the use of plasmon-pole models for the frequency dependence of the dielectric matrix. We provide well-converged numerical values for excitation energies of molecules and semiconducting solids, which may serve as benchmarks for other numerical techniques, and which allow one to establish the performance of many-body perturbation theory at the non self-consistent *GW* level, with respect to available experiments.

The rest of the paper is organized as follows: In section II we briefly summarize the theoretical background to compute quasiparticle energies based on the spectral decomposition of the static dielectric matrix, and we describe several numerical advantages of our approach. Section III presents calculations of ionization potentials (IPs) and electron affinities (EAs) of molecules, and comparisons of results to those of existing *GW* calculations. In section IV we provide data for ionization potentials of a large set of molecules, which may be used as benchmarks for future calculations. In section V, applications to extended systems are presented, including crystals and armorphous solids. Finally our conclusions and outlook are given in section VI.

II. THEORETICAL BACKGROUND

Within the framework of many-body perturbation theory, quasiparticle energies, E_n^{qp}, and wavefunctions, $\psi_n^{qp}(\mathbf{r})$, are obtained by solving the following quasiparticle equation:

$$[T + V_{ion}(\mathbf{r}) + V_H(\mathbf{r})]\psi_n^{qp}(\mathbf{r}) + \int d\mathbf{r}' \Sigma(\mathbf{r}, \mathbf{r}'; E_n^{qp})\psi_n^{qp}(\mathbf{r}') = E_n^{qp}\psi_n^{qp}(\mathbf{r}), \quad (1)$$

where T is the kinetic energy operator, $V_{ion}(\mathbf{r})$ is the external potential of the nuclei, $V_H(\mathbf{r})$ is the Hartree potential, and Σ is the non-local, energy-dependent, and non-Hermitian self-energy operator, which describes many-body electronic interactions.

In the *GW* approximation,[5] the self-energy is expressed in terms of the interacting one-electron Green's function G and the screened Coulomb interaction W:

$$\Sigma(\mathbf{r}, \mathbf{r}'; i\omega) = \frac{1}{2\pi} \int d\omega' G(\mathbf{r}, \mathbf{r}'; i(\omega - \omega'))W(\mathbf{r}, \mathbf{r}'; i\omega'), \quad (2)$$

where $W = \epsilon^{-1} \cdot v_c$, ϵ is the dielectric matrix, and v_c is the bare Coulomb potential.

In most practical implementations of the *GW* method, the one-electron Green's function is approximated by the non-interacting one, G°, evaluated using eigenvalues, ε_n, and wavefunctions, ψ_n, obtained from Kohn-Sham (KS) Hamiltonians:

$$G^\circ(\mathbf{r}, \mathbf{r}', i\omega) = \sum_n \frac{\psi_n(\mathbf{r})\psi_n^*(\mathbf{r}')}{i\omega - \varepsilon_n}. \quad (3)$$

The screened Coulomb interaction W° is computed within the random phase approximation (RPA):

$$W^\circ = \epsilon^{-1} \cdot v_c = v_c + v_c \cdot \chi \cdot v_c, \quad (4)$$

where ϵ^{-1} denotes the inverse RPA dielectric matrix, and χ is the interacting density-density response function. In the current notation $v_c \cdot \chi = \int d\mathbf{r}'' v_c(\mathbf{r}, \mathbf{r}'')\chi(\mathbf{r}'', \mathbf{r}'; i\omega)$, and similarly for all other quantities. Within the RPA, χ is related to the non-interacting density-density response function, χ°, by the equation: $\chi = (1 - \chi^\circ \cdot v_c)^{-1} \cdot \chi^\circ$, and χ° is written in terms of KS eigenvalues and orbitals:

$$\chi^\circ(\mathbf{r}, \mathbf{r}'; i\omega) = 4\ \mathrm{Re} \sum_{cv} \frac{\psi_v^*(\mathbf{r})\psi_c(\mathbf{r})\psi_c^*(\mathbf{r}')\psi_v(\mathbf{r}')}{i\omega - (\varepsilon_c - \varepsilon_v)}, \quad (5)$$

where the subscripts v and c indicate valence and conduction states, respectively (or occupied and virtual states in the case of molecules). Within first-order perturbation theory, quasiparticle energies (QPEs) are obtained as corrections to the unperturbed KS eigenvalues:

$$E_n^{qp} = \varepsilon_n + \langle\psi_n|\Sigma_{G^\circ W^\circ}(E_n^{qp})|\psi_n\rangle - \langle\psi_n|V_{xc}|\psi_n\rangle, \quad (6)$$

where V_{xc} is the exchange-correction potential entering the chosen KS Hamiltonian.

A. Conventional *GW* approach

In conventional *GW* calculations,[6] one computes the non-interacting Green's function $G^\circ(\mathbf{r}, \mathbf{r}'; i\omega)$ and the density-density response function $\chi^\circ(\mathbf{r}, \mathbf{r}'; i\omega)$ directly from the expressions of Eq. (3) and Eq. (5), respectively. This approach thus requires a summation over both occupied and unoccupied orbitals, hereafter refered to as the sum-over-states (SOS) approach. Despite being widely used, there are serious technical difficulties that limit its applicability to systems with more than a few tens of atoms.

First, a large number of unoccupied states is usually required to converge QPEs.[10–13] Even for molecules with a few atoms, several thousands of unoccupied states might be required. Due to this slow convergence, an extrapolation scheme is often employed to obtain QPEs in the limit of infinite number of unoccupied states.[13,18] However, the final result may depend on the specific function used in the extrapolation procedure.

Second, since the inverse dielectric matrix ϵ^{-1} enters the calculation of the screened Coulomb interaction W° (Eq. 4), if one evaluate ϵ directly from the expression of χ_0 in Eq. 5 then ϵ must be stored and inverted. As a result, large computational resources, in terms of both memory and CPU time, are usually required in practical applications. In many cases, the size of the dielectric matrix is truncated to make the calculation numerically affordable. Often, a cutoff energy of a few Ry is employed (much smaller than that adopted for the KS wavefunctions) when using a plane-wave basis set to represent the

dielectric matrix, leading to a significant reduction of the computational resources. However, this approximation may lead to incorrect converged results of QPEs as shown in the case of ZnO.[11]

Furthermore, in the conventional *GW* approach, the frequency dependence of the dielectric matrix is often approximated by various plasmon-pole models.[6,19–21] This approximation not only reduces the computational workload, but also provides an analytical expression for the self-energy as a function of frequency. However, it has been shown that results obtained with different plasmon-pole models may be significantly different,[8,22] and thus it is important to develop efficient techniques to explicitly take into account the frequency dependence of W.

In the following, we present in detail the scheme we proposed in Ref. 14 to compute QPEs, which avoids all the difficulties mentioned above.

B. *GW* calculations from a spectral decomposition of the static dielectric matrix

The self-energy in Eq. (2) can be written as a sum of an exchange, Σ_x, and a correlation, Σ_c, term. Within a plane-wave, pseudopotential formulation, the exchange term is evaluated with the techniques of Refs. 23, while Σ_c can be written as:

$$\Sigma_c = G^\circ(v_c^{\frac{1}{2}} \cdot \overline{\chi} \cdot v_c^{\frac{1}{2}}) = G^\circ(v_c^{\frac{1}{2}} \cdot (\tilde{\epsilon}^{-1} - 1) \cdot v_c^{\frac{1}{2}}), \quad (7)$$

where $\overline{\chi} = v_c^{\frac{1}{2}} \cdot \chi \cdot v_c^{\frac{1}{2}}$ is the symmetrized interacting density-density response function, and $\tilde{\epsilon} = v_c^{-\frac{1}{2}} \cdot \epsilon \cdot v_c^{\frac{1}{2}}$ is the Hermitian dielectric matrix.

We use a spectral decomposition to represent the inverse of the static Hermitian dielectric matrix:[24]

$$\tilde{\epsilon}^{-1}(\mathbf{r},\mathbf{r}') - 1 \equiv \overline{\chi}(\mathbf{r},\mathbf{r}') = \sum_i^{N_{eig}} (\lambda_i^{-1} - 1)\Phi_i^*(\mathbf{r})\Phi_i(\mathbf{r}'), \quad (8)$$

where λ_i and $\Phi_i(\mathbf{r})$ denote eigenvalues and eigenvectors of $\tilde{\epsilon}(\mathbf{r},\mathbf{r}')$. These dielectric eigenvectors $\{\Phi_i(\mathbf{r})\}$ are then used as a basis to expand the frequency dependent dielectric matrix and density-density response function:

$$\tilde{\epsilon}^{-1}(\mathbf{r},\mathbf{r}',i\omega) - 1 \equiv \overline{\chi}(\mathbf{r},\mathbf{r}';i\omega) = \sum_{i,j=1}^{N_{eig}} \overline{c}_{ij}(i\omega)\Phi_i^*(\mathbf{r})\Phi_j(\mathbf{r}'), \quad (9)$$

where $\overline{c}_{ij}$ are expansion coefficients.

Finally the expectation value of the correlation self-energy (Eq. 7) in the imaginary frequency domain for any KS state is:

$$\langle\psi_n|\Sigma_c(i\omega)|\psi_n\rangle = \frac{1}{2\pi}\sum_{i,j=1}^{N_{eig}} \int d\omega'\ \overline{c}_{ij}(i\omega')\langle\psi_n(v_c^{\frac{1}{2}}\Phi_i)|(\widehat{\mathrm{H}}^\circ - i(\omega-\omega'))^{-1}|\psi_n(v_c^{\frac{1}{2}}\Phi_j)\rangle, \quad (10)$$

where $|\psi_n(v_c^{\frac{1}{2}}\Phi_j)\rangle$ is a vector whose coordinate representation is $\langle\mathbf{r}|\psi_n(v_c^{\frac{1}{2}}\Phi_j)\rangle = \psi_n(\mathbf{r})\int d\mathbf{r}' v_c^{\frac{1}{2}}(\mathbf{r},\mathbf{r}')\Phi_j(\mathbf{r}')$, and $\widehat{\mathrm{H}}^\circ$ is the unperturbed KS Hamiltonian.

The method to compute the correlation self-energy presented here offers several advantages: (i) dielectric eigenvectors $\{\Phi_i(\mathbf{r})\}$ and therefore the dielectric matrix can be constructed without explicit calculations of unoccupied electronic states by using density functional perturbation theory and iterative diagonalization algorithms;[24] (ii) in constrast to plane-wave representations of $\tilde{\epsilon}$, the evaluation of a large dielectric matrix is avoided, as a relatively small number of eigenvectors N_{eig} is necessary to numerically converge the summation of Eq. (8);[24,25] (iii) the correlation self-energy $\Sigma_c(i\omega)$ over a wide frequency range is evaluated by the Lanczos algorithm,[26] and its value in the real frequency domain is then obtained by analytical continuation methods,[27,28] thus no plasmon-pole model is needed. Details of the iterative calculations of dielectric eigenvectors and the Lanczos algorithm can be found in Appendix A and B, respectively. We implemented this scheme for norm-conserving pseudopotentials as a postprocessing module in the Quantum Espresso distribution.[29]

C. Basis functions for the dielectric matrix

An important step in our calculations is the construction of the basis functions $\{\Phi_i(\mathbf{r})\}$ to represent the inverse

TABLE I. Ionization potential (IP) and electron affinity (EA) (eV) of the benzene molecule computed for different convergence thresholds in the iterative procedure used to iteratively diagonalize the dielectric matrix.

Threshold	10^{-6}	10^{-3}	10^{-2}	10^{-1}
IP	9.22	9.22	9.21	9.20
EA	-0.81	-0.81	-0.81	-0.82

of the Hermitian dielectric matrix (Eq. 8). In principle, any complete set of functions may be employed, and several choices have been claimed to improve the efficiency of calculations, with respect to plane-waves.[10,15] Our choice of dielectric eigenvectors at $i\omega = 0$ as a polarization basis set is not only physically sound but also practically convenient, as only one convergence parameter (N_{eig}) is involved.

In the iterative procedure chosen for the spectral decomposition of the dielectric matrix (Eq. 8), any dielectric eigenvector is considered to be converged when the change of the corresponding eigenvalue in two successive iterations is less than a given threshold. When the dielectric eigenvalues are used for calculations of RPA correlation energies of weakly bound van der Waals systems, a threshold as small as 10^{-5} or 10^{-6} (in Rydberg atomic units) is necessary to converge the energy within a few meV (typical energy scale of van der Waals interactions).[30,31] Instead, in *GW* calculations, we found that much larger thresholds are sufficient to obtain converged QPEs.

An example is given in Table I for the case of the benzene molecule,[32] where the computed values of the IP and EA show a variation of only 0.02 eV when the threshold increases from 10^{-6} to 10^{-1}. These results indicate that linear spaces spanned by eigenvectors computed with different thresholds are basically the same, leading to very small differences in the computed QPEs. This represents a significant advantage, as one can save considerable amount of CPU time by using eigenvectors obtained with relatively large thresholds without compromising the accuracy of the calculated QPEs.

D. Computational cost

We now turn to a discussion of the efficiency of the method presented in II. B and II. C. We denote by N_v and N_c the number of valence and conduction bands, and by $N_{pw\psi}$ and $N_{pw\overline{\chi}}$ the number of plane-waves used to represent wavefunctions and the response function $\overline{\chi}$ (and the dielectric matrix), respectively. The computational workload[23,24] to generate the dielectric matrix with N_{eig} eigenvectors scales as $N_{iter} \times N_{eig} \times N_{pw\psi} \times N_v^2$ with N_{iter} being the number of iterations needed to converge dielectric eigenvectors in iterative diagonalization procedures (N_{iter} is typically not larger than 10 in all cases considered here). In addition, the cost of Lanczos chains generation is $N_{Lanczos} \times N_{eig} \times N_{pw\psi} \times N_v^2$ where $N_{Lanczos}$ is the number of Lanczos iterations (see Appendix B), which is typically just a few tens. Therefore the total workload of our approach is $(N_{iter} + N_{Lanczos}) \times N_{eig} \times N_{pw\psi} \times N_v^2$, and it is proportional to the fourth power of the system size.

This workload represents a substantial improvement over that of conventional approaches, $N_{pw\overline{\chi}}^2 \times N_v \times N_c$, which is also proportional to the fourth power of the system size, but with a substantially larger prefactor. In particular, $N_{pw\psi}$ is much smaller than $N_{pw\overline{\chi}}$: $N_{pw\overline{\chi}}$ is used to represent density responses and perturbing potentials, whose kinetic-energy cutoff is four times as large as that needed to represent wavefunctions, in the case of norm-conserving pseudopotentials. Furthermore, the number of occupied states N_v is often an order of magnitude smaller than the number of unoccupied states N_c required to converge summations in the dielectric matrix and Green's function; instead the sum $(N_{iter} + N_{Lanczos})$ is usually less than a few tens, as mentioned above. Finally, the number of eigenvectors N_{eig} is usually several orders of magnitude smaller than the size of the response function $N_{pw\overline{\chi}}$.

Taking the benzene molecule as an example to illustrate the efficiency of our appoach, we found that the use of $N_{eig} = 300$ and $N_{Lanczos} = 25$ is sufficient to obtain well converged values of QPEs within 0.05 eV. For calculations using a kinetic energy cutoff of 40 Ry for the wavefunction and a cell size of $L = 25$ a.u., in the SOS approach, the number of basis functions for the dielectric matrix and wavefunctions are $N_{pw\overline{\chi}} \sim 5.3 \times 10^5$ and $N_{pw\psi} \sim 6.6 \times 10^4$, respectively. Taking $N_v = 15$ and $N_c \sim 2.6 \times 10^3$,[12] we estimate that the computational cost of our method is about four order of magnitude smaller than that of the conventional SOS. Such an efficiency allowed us to compute QPEs of systems with hundreds of valence electrons.[14,33]

III. COMPARISON WITH PREVIOUS *GW* CALCULATIONS

A. Comparison with plane-wave basis set calculations

In order to illustrate the importance of converging the number of unoccupied states in *GW* calculations, in this section we compare QPEs obtained with the current method to those using the conventional plane-wave based SOS approach. Two systems were selected, the benzene diamine-$C_6H_8N_2$ (BDA) molecule and C_{60}, for which SOS's results of the IP and EA have been reported in the literature.[12,13]

1. Benzene diamine molecule

The conventional $G^\circ W^\circ$ approach that requires sums over unoccupied states was employed in Ref. 13 to investigate the BDA molecule. In order to directly compare with this work, we adopted the Perdew-Burke-Ernzerhof (PBE) exchange-correlation functional[34] with a plane-wave cutoff of 60 Ry, and periodic boundary conditions with a cell of 30 a.u. The equilibrium geometry of the gas-phase BDA was determined using DFT with the PBE functional. We used $N_{eig} = 300$, which yields values of QPEs converged within 0.02 eV.

TABLE II. Ionization potential (IP) and electron affinity (EA) (eV) of the benzene diamine (BDA) molecule, as obtained from Kohn-Sham eigenvalues (PBE-eig), and from GW calculations at different levels of theory. G^1W^1 corresponds to calculations where both G and W are updated using the QPEs from the previous cycle, while only W is updated in the $G^\circ W^1$ calculation. The number of unoccupied states (N_c) included in conventional GW calculations is also given.

		No. of unocc. orb	IP	EA
Ref. 13				
	PBE-eig	$\cdots$	4.22	1.03
	$G^\circ W^\circ$	N_c=1024	5.89	-2.18
	$G^\circ W^\circ$	$N_c \to \infty$	6.64	-1.42
	$G^\circ W^1$	$N_c \to \infty$	6.71	-1.65
	G^1W^1	$N_c \to \infty$	6.85	-1.59
This work				
	PBE-eig	$\cdots$	4.21	1.02
	$G^\circ W^\circ$	$\cdots$	6.88	-1.02
Expt.[35]		$\cdots$	7.34	$\cdots$

Table II summarizes the IP and EA for the gas phase BDA, computed at different levels of theory. Consistent with previous work,[13] the IP computed at the DFT/PBE level of theory (PBE-eig) underestimates the experimental value by 3.12 eV. Our $G^\circ W^\circ$ calculations significantly improve the IP value, with the error relative to experiment reduced to 0.46 eV.

The slow convergence of QPEs of the BDA molecule with respect to the number of unoccupied states has been discussed in Ref. 13. In particular, at the $G^\circ W^\circ$ level of theory, when 1024 unoccupied states are included, the computed IP shows a deviation as large as 0.75 eV compared with the $N_c \to \infty$ extrapolated value. Extrapolating the calculated values of IP to infinite N_c reduces the error with respect to experiment from 1.45 eV to 0.7 eV, and depending on whether G or W is updated using the QPEs from the previous cycle, this error may be further reduced to 0.5 eV.

At the $G^\circ W^\circ$ level of theory, our result for the IP is higher and closer to experiment than the extrapolated value reported in Ref. 13. The discrepancy may be attributed to the use of a relatively small cutoff for the dielectric matrix (6.0 Ry), as well as the use of a plasmon-pole model.[13] Additional errors may stem from the choice of the analytical form of the function used to extrapolate the value of IP to infinite N_c. Similar to the IP, our $G^\circ W^\circ$ result for EA is higher than the extrapolated value reported in Ref. 13; unfortunately no experimental value for EA of the BDA molecule is available.

TABLE III. Ionization potential (IP) and electron affinity (EA) (eV) for buckminsterfullerene (C_{60}) as obtained from Kohn-Sham eigenvalues (PBE-eig), and from $G^\circ W^\circ$ calculations. The number of unoccupied states (N_c) included in conventional GW calculations is also given. SAPO stands for simple approximate physical orbitals.[12]

		No. of unocc. orb	IP	EA
Ref. 12				
	PBE-eig	$\cdots$	5.84	4.19
	$G^\circ W^\circ$	N_c=5370	6.76	2.19
	$G^\circ W^\circ$	27387 SAPOs	7.21	2.62
This work				
	PBE-eig	$\cdots$	5.81	4.13
	$G^\circ W^\circ$	$\cdots$	7.31	2.74
Expt.[35]		$\cdots$	7.64	2.69

2. *Buckminsterfullerene C_{60}*

For buckminsterfullerene C_{60}, we employed the PBE exchange-correlation functional with a plane-wave cutoff of 40 Ry, and periodic boundary conditions with a cell of 40 a.u.. Our computed values of IP and EA at the DFT/PBE level of theory are in excellent agreement with previous studies[12] (see Table III). QPEs of C_{60} were calculated using $N_{eig} = 700$, that yields converged values of IP and EA within 0.03 eV.

Calculations of QPEs of C_{60} using the conventional $G^\circ W^\circ$ approach showed a slow convergence with respect to the number of unoccupied states.[12] In particular, using 5370 unoccupied states, the values of the IP and EA are strongly underestimated compared to experiment, with errors of 0.88 eV and 0.51 eV, respectively. In contrast, with the current approach that avoids the direct evaluation of unoccupied states, we found values of 7.31 eV and 2.74 eV for the IP and EA, respectively, in good agreement with experiment (within 0.30 eV).

The authors of Ref. 12 also addressed the problem of the computational cost associated with the construction of unoccupied states in $G^\circ W^\circ$ calculations, and proposed to replace the DFT unoccupied states with simple approximate physical orbitals (SAPOs) that are computationally cheaper to generate. As shown in Table III, our results for EA and IP are in good agreement with those reported in Ref. 12 when a large number of SAPOs (27387) is included in $G^\circ W^\circ$ calculations. We note that the approach of Ref. 12 still requires to carry out explicit sums over SAPOs, and the use of a plasmon-pole model together with a relatively small energy cutoff (6.0 Ry) to represent the dielectric matrix.

TABLE IV. Ionization potentials (IP), electron affinities (EA), and quasiparticle gaps (eV) for a set of molecules (see text) as obtained from Kohn-Sham eigenvalues (LDA-eig), and from LDA based $G^\circ W^\circ$ calculations.

	LDA-eig		$G^\circ W^\circ$		Expt.[35]
	Present	Ref. 36	Present	Ref. 36	
$C_{14}H_{10}$					
IP	5.18	5.47	7.25 [a]	6.89	7.40
EA	2.81	3.22	1.05	0.74	0.50
Gap	2.37	2.25	6.20	6.15	6.90
$C_{18}H_{12}$					
IP	4.85	5.15	7.04	6.37	6.97
EA	3.19	3.58	1.41	1.34	1.07
Gap	1.66	1.57	5.63	5.03	5.90
$C_{22}H_{14}$					
IP	4.63	4.94	6.30	5.98	6.60
EA	3.47	3.84	1.96	1.77	1.40
Gap	1.16	1.10	4.34	4.21	5.20
C_{60}					
IP	6.03	6.37	7.45	7.28	7.64
EA	4.35	4.79	3.05	2.88	2.69
Gap	1.68	1.58	4.40	4.40	4.95
H_2Pc					
IP	5.21	5.56	6.11	6.08	6.40
EA	3.76	4.14	2.35	2.41	···
Gap	1.45	1.42	3.76	3.67	···

[a] A value of 6.65 eV was reported in Ref. 37 using a TZVPP Gaussian basis set and the PBE exchange-correlation functional.

B. Comparison with localized basis set calculations

Recently QPEs of several molecules of interest for photovoltaic applications were investigated within the *GW* approximation.[36] These calculations were based on the conventional implementation of the *GW* method with a localized basis-set and a direct sum over unoccupied states. In order to further validate our scheme, and to compare our results with those obtained with localized basis-sets, we computed QPEs for anthracene ($C_{14}H_{10}$), tetracene ($C_{18}H_{12}$), pentacene ($C_{22}H_{14}$), C_{60} and phthalocyanine-$C_{32}H_{18}N_8$ (H_2Pc) molecules, whose values were reported in Ref. 36.

Similar to Ref. 36, our calculations were performed with the local density approximation (LDA) for the exchange-correlation functional. A kinetic energy cutoff of 40 Ry for wavefunctions was employed for all systems, except for the H_2Pc molecule where we used 70 Ry due to the presence of the nitrogen atom. The size of the supercell was chosen in such a way that the distance between periodic images was at least 10 Å. The QPEs of C_{60}, whose number of valence electrons is the largest in this set of molecule, were computed using N_{eig}=700, similar to the calculations with the PBE functional (Table III). The number of dielectric eigenvectors needed to converge QPEs of other molecules was also carefully checked, e.g., using N_{eig}=600 yields values of the IP and EA converged within 0.05 eV for the case of H_2Pc.

The computed values of the IP, EA and quasiparticle gap obtained at different levels of theory are summarized in Table. IV. The IPs computed within the DFT/LDA (LDA-eig) significantly underestimate experimental values. In contrast, for molecules whose experimental EAs are available, we found that DFT-LDA overestimates experiments by ~ 2.0 eV. Calculations at the $G^\circ W^\circ$ level of theory show a significant improvement, bringing the errors of IP and EA to average values of 0.20 and 0.45 eV, respectively, in satisfactory agreement with experiments.

As seen in Table IV, our $G^\circ W^\circ$ results for IP and EA are overall larger than those obtained with localized basis-set, leading to better (worse) agreement of IP (EA) with experiment than those reported in Ref. 36. Quasiparticle gaps for this set of molecule, turned out to be in excellent agreement with the results of Ref. 36, yielding an average error of 0.60 eV compared to experiment.

Direct comparison with the $G^\circ W^\circ$ results reported in Ref. 36 is not straightforward, due to several technical differences. As shown in Table IV, there are already significant differences in the results of ground state calculations using localized basis sets and plane-waves. For all molecules studied here, we found that absolute values of LDA eigenvalues obtained with plane-waves are systematically smaller than those reported with a localized basis set by 0.30-0.40 eV. Such large differences cannot be attributed to the sole change in the relaxed geometries of the molecules. More importantly, these discrepancies are not negligible when compared, for example, to the quasiparticle corrections of 0.90 eV (this work) and 0.52 eV (Ref. 36) for IPs of H_2Pc, respectively.[38]

IV. IONIZATION POTENTIALS FOR THE TEST SET G2/97

In order to provide highly converged ionization potentials that can be used as a benchmark for future calculations, we considered a subset of 80 molecules from the G2/97 test set.[39] The open-shell molecules belonging to the G2/97 test set were not considered in this work. To minimize possible effects of molecular geometry on $G^\circ W^\circ$ calculations, we employed the relaxed geometries at the MP2 level of theory with the 6-31G(d) basis set as published in Ref. 39, without any further structural relaxation. In addition, we used PBE Troullier-Martins norm-conserving pseudopotentials taken from the Abinit distribution.[40] Therefore our results are straightforward to reproduce.

Together with the $G^\circ W^\circ$ method, we considered other approaches to evaluate the IP. First, IPs were obtained from the KS energies corresponding to the highest occu-

pied molecular orbital in DFT calculations. We considered not only the PBE approximation to the exchange-correlation potential but also fully nonlocal approximations, including Hartree-Fock (HF) and hybrid functionals. We choose two popular hybrid functionals, i.e., the PBE0[41] and the HSE06[42] ones, both of which contain 25% Fock exchange. All $G^\circ W^\circ$ calculations were performed using ground state PBE eigenvalues and orbitals.

We further evaluated IPs from total energy differences in a so-called delta self-consitent field (ΔSCF) procedure:

$$I = E_0^{N-1} - E_0^N, \tag{11}$$

where E_0^N is the total energy of the N electron system, that can be computed, e.g., with the PBE or hybrid exchange-correlation functionals.

Table V presents the IPs of 80 molecules computed within different approaches, together with experimental results. The mean error (ME) and mean absolute error (MAE) of the computed IPs with respect to experimental data are summarized in Fig. 1 and Table VI. We also report ME and MAE for three specific classes of molecules of the test set, specifically non-hydrogen systems, hydrocarbons, and substituted hydrocarbons. As well known, IPs obtained from the PBE-HOMO energies suffer from the self-interaction error,[43] and they thus strongly underestimate experiments (negative ME) with a MAE as large as 4.16 eV. Part of this self-interaction error is removed using the PBE0 and HSE06 functionals due to the inclusion of 25% Fock exchange. However the IPs obtained from the HSE06 and PBE0 eigenvalues are still far from experiment with MAEs of 3.13 eV and 2.73 eV, respectively.

Since screening is weak in small molecules and HF is self-interaction free, HF results are much closer to experiment, with a MAE of 0.79 eV. In general, IPs computed within HF overestimate experimental values (positive ME). The $G^\circ W^\circ$ approximation based on ground state PBE eigenvalues and orbitals performs better than HF, yielding a MAE of 0.40 eV with respect to experiments. This value is in agreement with those reported in Refs. 44 and 45. Therefore it appears that irrespective of the implementation, IPs obtained at the $G^\circ W^\circ$ level of theory, with PBE ground state eigenvalues and orbitals, show a MAE in the range of 0.4-0.5 eV, with respect to experiment. Not surprisingly, the ΔSCF procedure provides good quality IPs. We find that ΔSCF results with the PBE0 and HSE06 hybrid functionals perform equally well, with a MAE of 0.27 eV. They are superior to those based on the semilocal PBE exchange-correlation functional, with a MAE of 0.47 eV. We note that for some molecules, the ΔSCF procedure based on the PBE functional severely underestimates experiment, e.g., the deviation is as large as 1.58 eV for the BF_3 molecule. In such cases, the $G^\circ W^\circ$ approximation shows significant improvement over the PBE based ΔSCF, leading to very good agreement with the hybrid functionals based ΔSCF calculations.

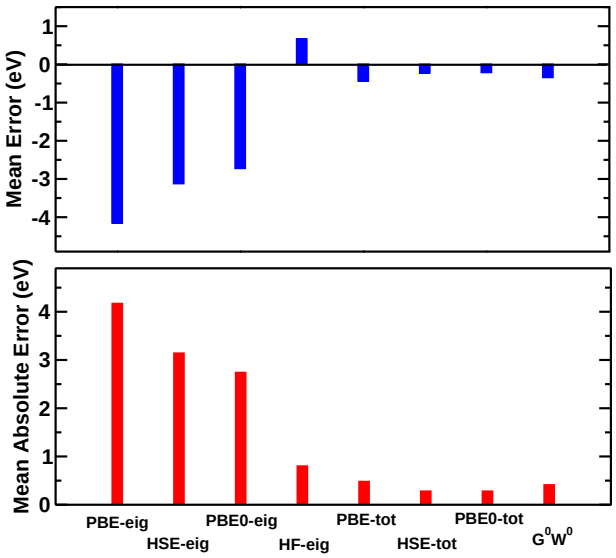

FIG. 1. Deviation of computed ionization potentials, obtained within different approaches (see text), with respect to experimental data. The upper panel shows the mean error (ME), and the lower panel the mean absolute error (MAE) for a 80 molecule set (see text). The grey rectangle corresponds to the MAE and ME computed for all the molecules of the set. The red, blue and green rectangles correspond to the results computed for non-hydrogen systems, hydrocarbons, and substituted hydrocarbons only, respectively.

For all approaches presented here, the hybrid functionals based ΔSCF performs the best for IPs when compared to experimental results. However, unlike the $G^\circ W^\circ$ approach, it does not allow one to access the full energy spectrum of the system and its generalization to extended systems is not straightforward, although approximate forms of ΔSCF for solids have been recently proposed in the literature.[46]

V. BAND GAPS OF SEMICONDUCTORS

In this section, we turn to extended systems and we consider different semiconductors whose QPEs have been reported in literature. In addition we present a study of the band gap of a disordered system represented by a 56 atoms supercell (256 valence electrons). Note that for the purpose of treating systems with large supercells, in the present work we sample the Brillouin zone using the Γ point only.

In extended systems, an accurate sampling of the Brillouin zone is necessary to compute the long-wavelength component of the dielectric matrix.[48] In the present work, the "head" of the dielectric matrix ($\mathbf{G} = \mathbf{G}' = 0$) at frequency $i\omega$ is computed separately using the Lanczos chain algorithm with dense k-point meshes. Note that when sampling the Brillouin zone with the Γ point only, the "wings" of the dielectric matrix ($\mathbf{G} = 0, \mathbf{G}' = 0$) vanish.[49]

TABLE V. Ionization potentials (eV) obtained at different levels of theory (see text), together with experimental results.[35] "X-eig" (with X=PBE, HSE, PBE0 and HF) refers to results obtained from the KS eigenvalues while "X-tot" corresponds to those computed with the ΔSCF procedure.

Molecule	PBE-eig	HSE-eig	PBE0-eig	HF-eig	PBE-tot	HSE-tot	PBE0-tot	$G^\circ W^\circ$	Expt.
Non-hydrogen systems									
BF_3	9.94	11.70	12.09	17.72	14.38	15.17	15.18	15.12[a]	15.96
BCl_3	7.49	8.51	8.91	12.27	10.75	11.30	11.26	11.37[b]	11.62
AlF_3	9.54	11.18	11.58	16.98	13.48	14.28	14.30	14.34	15.45
$AlCl_3$	7.77	8.77	9.17	12.49	10.83	11.36	11.39	11.59	12.01
CF_4	10.26	12.07	12.47	18.28	14.48	15.43	15.44	15.38	16.20
CCl_4	7.41	8.45	8.84	12.29	10.50	11.07	11.10	11.22	11.69
COS	7.40	8.22	8.61	11.37	11.19	11.23	11.24	11.01	11.19
CS_2	6.66	7.32	7.70	10.03	9.96	9.99	9.99	9.89	10.09
CF_2O	8.44	9.88	10.28	14.94	13.09	13.27	13.28	12.91	13.60
SiF_4	10.49	12.20	12.60	18.14	14.35	15.31	15.33	15.38	16.40
$SiCl_4$	7.87	8.89	9.28	12.64	10.83	11.43	11.46	11.58	12.06
N_2O	8.28	9.29	9.68	13.09	12.66	12.66	12.67	12.23	12.89
ClNO	7.35	8.26	8.65	11.55	11.22	11.25	11.25	11.29	10.94
NF_3	8.52	9.95	10.35	15.10	13.03	13.44	13.44	13.07	13.60
PF_3	7.86	8.86	9.25	12.67	11.81	12.06	12.07	11.85	12.20
O_3	7.98	9.46	9.86	13.11	12.58	12.30	12.30	12.20	12.73
F_2O	7.63	9.41	9.81	15.58	12.63	13.18	13.18	12.75	13.26
ClF	7.83	9.05	9.45	13.41	12.41	12.65	12.66	12.62[c]	12.77
C_2F_4	6.12	7.14	7.54	10.81	9.99	10.26	10.27	10.08	10.69
C_2Cl_4	5.91	6.66	7.05	9.60	8.89	9.15	9.16	9.07	9.50
CF_3CN	9.38	10.43	10.83	14.01	13.36	13.68	13.69	13.3	14.30
Hydrocarbons									
C_3H_4 (propyne)	6.40	7.21	7.61	10.29	10.11	10.11	10.12	10.00	10.37
C_3H_4 (allene)	6.48	7.25	7.65	10.19	9.95	9.97	9.98	9.82	10.00
C_3H_4 (cyclopropene)	6.00	6.74	7.13	9.58	9.62	9.62	9.63	9.67	9.86
C_3H_6 (propylene)	6.15	6.89	7.26	9.64	9.65	9.62	9.63	9.51	9.91
C_3H_6 (cyclopropane)	7.00	7.90	8.30	11.32	10.68	10.74	10.74	10.60	10.54
C_3H_8 (propane)	7.65	8.67	9.06	12.62	11.08	11.49	11.50	11.84[d]	11.51
C_4H_6 (butadiene)	5.73	6.31	6.69	8.66	8.82	8.79	8.79	8.68	9.03
C_4H_6 (2-butyne)	5.80	6.59	6.99	9.64	8.19	9.31	9.31	9.25	9.79
C_4H_6 (methylene)	6.18	6.90	7.30	9.69	9.58	9.54	9.55	9.42	9.60
C_4H_6 (bicyclobutane)	5.68	6.44	6.84	9.43	9.07	9.11	9.12	9.05	8.70
C_4H_6 (cyclobutene)	5.93	6.63	7.02	9.35	9.33	9.31	9.32	9.25	9.59
C_4H_8 (cyclobutane)	7.13	8.08	8.48	11.74	10.52	10.76	10.78	10.81	10.7
C_4H_8 (isobutene)	5.81	6.51	6.91	9.26	9.11	9.10	9.11	9.04	9.41
C_4H_{10} (transbutane)	7.48	8.48	8.88	12.27	10.64	11.08	11.09	11.58[e]	11.09
C_4H_{10} (isobutane)	7.50	8.48	8.87	12.33	10.79	11.16	11.18	11.57[f]	11.13
C_5H_8 (spiropentane)	6.40	7.22	7.62	10.39	9.56	9.76	9.78	9.62	9.73
C_6H_6	6.18	6.76	7.15	8.98	9.21	9.20	9.21	9.04[g]	9.23

[a] A $G^\circ W^\circ$ value of 15.21 eV was reported in Ref. 47.
[b] A $G^\circ W^\circ$ value of 11.25 eV was reported in Ref. 47.
[c] A $G^\circ W^\circ$ value of 10.72 eV was reported in Ref. 47.
[d] A $G^\circ W^\circ$ value of 11.60 eV was reported in Ref. 37.
[e] A $G^\circ W^\circ$ value of 11.16 eV was reported in Ref. 37.
[f] A $G^\circ W^\circ$ value of 11.19 eV was reported in Ref. 37.
[g] $G^\circ W^\circ$ values of 9.00 and 8.65 eV were reported in Ref. 37 and Ref. 47, respectively.

TABLE V. Continued.

Molecule	PBE-eig	HSE-eig	PBE0-eig	HF-eig	PBE-tot	HSE-tot	PBE0-tot	$G^\circ W^\circ$	Expt.
Substituted hydrocarbons									
CH_2F_2	8.09	9.50	9.90	14.48	12.41	12.94	12.95	13.05	13.27
CHF_3	9.46	10.93	11.33	16.12	13.71	14.34	14.35	14.34	14.80
CH_2Cl_2	7.18	8.19	8.59	11.99	10.61	11.03	11.05	11.25	11.40
$CHCl_3$	7.29	8.31	8.70	12.01	10.55	11.03	11.05	11.18	11.50
CH_3NH_2	5.39	6.47	6.87	10.59	9.5	9.53	9.54	9.02	9.65
CH_3CN	7.93	8.87	9.27	12.30	11.95	11.98	11.99	11.75	12.46
CH_3NO_2	6.82	8.23	8.63	12.30	10.97	11.36	11.37	10.71	11.29
CH_3ONO	6.48	7.74	8.13	12.39	10.63	10.84	10.85	9.95	10.44
CH_3SiH_3	7.81	8.72	9.11	12.29	11.24	11.48	11.49	11.35	11.6
HCOOH	6.88	8.12	8.52	12.74	11.25	11.26	11.27	11.06	11.5
$HCOOCH_3$	6.61	7.86	8.26	12.48	10.78	10.84	10.85	10.38	11.0
CH_3CONH_2	5.66	6.87	7.27	11.17	9.62	9.66	9.67	9.40	10.0
C_2H_4NH	5.77	6.81	7.21	10.63	9.67	9.71	9.72	9.48	9.85
NCCN	9.10	9.96	10.35	13.14	12.85	12.93	12.93	12.59	13.51
$(CH_3)_2NH$	4.99	6.00	6.39	9.96	8.74	8.78	8.79	8.63	8.95
CH_3CH2NH_2	5.37	6.43	6.83	10.48	9.25	9.31	9.32	9.02	9.50
CH_2CO	5.88	6.72	7.11	9.92	9.69	9.70	9.71	9.48	9.64
C_2H_4O	6.18	7.45	7.85	12.12	10.40	10.43	10.44	10.24	10.57
CH_3CHO	5.87	7.06	7.45	11.49	9.98	10.03	10.04	9.77	10.24
HCOCOH	6.30	7.49	7.88	11.95	10.02	10.46	10.47	10.22	10.60
CH_3CH_2OH	6.13	7.36	7.76	11.89	10.18	10.42	10.43	10.32	10.64
CH_3OCH_3	5.80	6.97	7.37	11.40	9.73	9.86	9.87	9.82	10.0
C_2H_4S	5.24	6.08	6.47	9.32	8.87	8.89	8.90	8.90[a]	9.0
$(CH_3)_2SO$	5.26	6.19	6.59	9.88	8.81	8.85	8.86	8.62	9.11
C_2H_5SH	5.42	6.25	6.65	9.54	9.05	9.01	9.11	9.02	9.28
CH_3SCH_3	4.96	5.77	6.16	9.02	8.46	8.52	8.53	8.58	8.67
CH_2=CHF	6.47	7.30	7.70	10.37	10.32	10.33	10.33	10.18	10.56
C_2H_5Cl	6.84	7.84	8.24	11.60	10.62	10.86	10.87	10.88	11.06
CH_2=CHCl	6.32	7.08	7.47	9.98	9.78	9.86	9.87	9.82	10.2
CH2=CHCN	7.20	7.90	8.29	10.64	10.59	10.61	10.62	10.50	11.1
CH_3COCH_3	5.55	6.74	7.14	11.11	9.43	9.51	9.52	9.48	9.8
CH_3COOH	6.43	7.67	8.07	12.23	10.51	10.59	10.60	10.27	10.9
CH_3COF	7.24	8.52	8.92	13.18	11.47	11.56	11.57	11.11	11.51
CH_3COCl	6.95	8.06	8.46	12.17	10.69	10.83	10.84	10.71	11.03
$CH_3CH_2CH_2Cl$	6.78	7.78	8.18	11.49	10.35	10.64	10.66	10.76	10.88
$(CH3)_2CHOH$	6.08	7.30	7.69	11.71	9.91	10.17	10.18	10.06	10.44
$C_2H_5OCH_3$	5.71	6.88	7.27	11.27	9.47	9.65	9.66	9.52	9.72
$(CH_3)_3N$	4.81	5.75	6.14	9.55	8.28	8.31	8.32	8.27	8.54
C_4H_4O	5.53	6.15	6.54	8.53	8.82	8.77	8.77	8.54	8.90
C_4H_4S	5.70	6.32	6.71	8.69	8.82	8.80	8.80	8.49	8.85
C_4H_5N	5.02	5.61	6.00	7.93	8.21	8.15	8.16	7.91	8.23
C_5H_5N	5.79	6.94	7.34	9.29	9.31	9.47	9.48	9.54	9.51

[a] A $G^\circ W^\circ$ value of 8.71 eV was reported in Ref. 47.

TABLE VI. Mean error (ME) and mean absolute error (MAE) of the computed ionization potentials (eV) reported in Table V with respect to experimental data.[35] Results for three specific classes of molecules are also presented.

Molecule	PBE-eig	HSE-eig	PBE0-eig	HF-eig	PBE-tot	HSE-tot	PBE0-tot	$G^\circ W^\circ$
Non-hydrogen systems								
ME	-4.72	-3.50	-3.10	0.81	-0.80	-0.41	-0.40	-0.52
MAE	4.72	3.50	3.10	0.84	0.82	0.45	0.44	0.55
Hydrocarbons								
ME	-3.57	-2.77	-2.38	0.31	-0.25	-0.09	-0.08	-0.08
MAE	3.57	2.77	2.38	0.52	0.31	0.18	0.17	0.29
Substituted hydrocarbons								
ME	-4.42	-3.13	-2.68	0.53	-0.22	-0.19	-0.16	-0.31
MAE	4.42	3.13	2.68	0.97	0.41	0.25	0.24	0.37
Total								
ME	-4.16	-3.13	-2.73	0.67	-0.44	-0.23	-0.22	-0.35
MAE	4.16	3.13	2.73	0.79	0.47	0.27	0.27	0.40

A. Quasiparticle energies of Si, AlAs and SiC

We considered Si first, which has been extensively studied by the electronic structure community, and for which several *GW* results are available. In addition, we present results for AlAs, a medium-gap semiconductor, and for SiC, a wide-gap semiconductor. We used a kinetic energy cutoff of 25 Ry for Si; 40 Ry for AlAs and SiC. Experimental lattice constants of 10.26 a.u. for Si; and 10.67 a.u. and 8.24 a.u. for AlAs and SiC were used, respectively. For all systems we employed a 64-atom cubic supercell and we sampled the corresponding Brilloun zone using the Γ point. The "head" of the dielectric matrix at the frequency $i\omega$ was computed with a 4×4×4 k-point grid. In order to compare to available *GW* calculations, we used the LDA exchange-correlation functional. Similar to calculations for molecules, we find that QPEs are converged with a relatively small number of Lanczos iterations (∼20-25). For all systems considered here, the QPEs were converged within 0.05 eV when using 600 dielectric eigenpotentials.

Table VIII presents the calculated QPEs at points of high-symmetry for Si, together with available theoretical and experimental results. For all energy bands, our results are in excellent agreement with those of other calculations using pseudopotentials, and plane-wave basis set, and full frequency integration (no plasmon-pole models).[10,28,50] In the vicinity of the valence band maximum (VBM) our results are also consistent with those obtained with plasmon-pole models.[51,52] However, as one moves away from the VBM, significant differences are found, e.g., our computed valence-band width is 11.64 eV, while it is 11.90-11.95 eV when using plasmon-pole models. These large deviations are not surprising, in fact, for Si the same behavior was observed with conventional *GW* approaches, when comparing QPEs obtained with plasmon-pole models and those with the contour deformation method that takes into account the full frequency dependence of the screened Coulomb interaction.[53] Our computed value of the valence-band width is in excellent agreement with that reported in Ref. 53 using the contour deformation method (11.7 eV).

Except for the energy band X_{1c}, our results are also in good agreement with those using the all-electron full-potential projector augmented wave method (PAW).[54] In addition, the consistency between our results and all other pseudopotential based calculations indicates that the large deviation (∼0.35 eV for X_{1c}) from Ref. 54 may stem from the contribution of core-electrons that are explicitly taken into account in PAW calculations.[54] Computed QPEs for AlAs and SiC are shown in Table IX and X, respectively. For AlAs our results are in good agreement with those using pseudopotentials with a plasmon-pole model, indicating that at least for AlAs, plasmon-pole models are a good approximation for the frequency dependence of the dielectric matrix. In constrast, for SiC, when comparing to results obtained with plasmon-pole models, we find small deviations in the vicinity of the VBM, but large variations away from the VBM. Similar to the case of Si, when compared to all-electron PAW approach, large variations (∼0.5 eV) are observed for the energy band X_{1c} of both AlAs and SiC.

Based on our observations, we conclude that using plasmon-pole models may be a good approximation only for energy levels close to the band gap. For all systems considered here, the convergence of QPEs with respect to the number of unoccupied states, as well as to the cutoff of the dielectric matrix does not appear to be as severe as, e.g. in the case of ZnO.[11]

TABLE VIII. Calculated quasiparticle energies at points of high-symmetry for Si (in eV), together with available theoretical and experimental results (as quoted in Ref. 28). Unless noted otherwise in the "Comment" row, all calculations use pseudopotentials, plane-waves, and no plasmon-pole models (PPM). GO stands for Gaussian orbitals and PAW for all electron full-potential projector augmented wave. Energies are measured relative to the valence band maximum.

	Present	Ref. 10	Ref. 28	Ref. 50	Ref. 51	Ref. 52	Ref. 54	Expt.
Γ_{1v}	-11.64	-11.49	-11.57	-11.57	-11.90	-11.95	-11.85	-12.5±0.6
Γ'_{25c}	0.0	0.0	0.0	0.0	0.0	0.0	0.0	0.0
Γ_{15c}	3.25	3.24	3.24	3.23	3.25	3.36	3.09	3.40, 3.05
Γ'_{2c}	3.92	3.89	3.94	3.96	3.86	3.89	4.05	4.23, 4.1
X_{1v}	-7.75	-7.58	-7.67	-7.57	-7.90	-7.95	-7.74	
X_{4v}	-2.88	-2.80	-2.80	-2.83	-2.96	-2.93	-2.90	-2.90, -3.3±0.2
X_{1c}	1.36	1.41	1.34	1.35	1.31	1.43	1.01	1.25
L'_{2v}	-9.38		-9.39	-9.35	-9.65	-9.70	-9.57	-9.3±0.4
L_{1v}	-6.93		-6.86	-6.78	-7.13	-7.14	-6.97	-6.7±0.2
L'_{3v}	-1.23		-1.17	-1.20	-1.25	-1.25	-1.16	-1.2±0.2
L_{1c}	2.21		2.14	2.18	2.13	2.19	2.05	2.1, 2.4±0.1
L_{3c}	4.00		4.05	4.06	4.13	4.08	3.83	4.15±0.1
Comment					PPM	GO/PPM	PAW	

B. Band gaps of amorphous Si_3N_4

As a final example, we present calculations of the quasiparticle band gap of amorphous Si_3N_4. We considered a model containing 56 atoms (256 valence electrons), taken from Ref. 55, whose structural and dielectric properties are in good agreement with experiments.[55,56] For $G^\circ W^\circ$ calculations, we used the PBE exchange-correlation functional with a kinetic energy cutoff of 60 Ry. The Brillouin zone was sampled with the Γ point only. We used 600 dielectric eigenpotentials to compute the quasiparticle band gap.

The band gap of amorphous Si_3N_4 measured in experiment is sensitive to the preparation procedure, with values ranging from 4.5 to 5.3 eV.[57] Within the $G^\circ W^\circ$ approximation, we obtained 4.87 eV for the band gap of amorphous Si_3N_4, that falls within the range of the experimental results. As expected, the band gap computed at the PBE level of theory is a strong underestimation of experiments (3.17 eV).

We also computed the band gap of our model with the HSE06 and PBE0 hybrid functionals and obtained values of 4.55 and 5.32 eV, respectively. It turns out that due to the large variation in the measured values, both $G^\circ W^\circ$ and hybrid functional approaches give results in resonable agreement with experiments. However, we note that in general, even if HSE06 and PBE0 hybrid functionals may provide good results for band gap calculations, they can fail for the interface or nanostructures calculations of the same materials.[7] In such cases, the GW approximation is required to provide reliable quantities such as band offsets or band alignments.

VI. CONCLUSIONS

In summary, we have presented an approach to perform $G^\circ W^\circ$ quasiparticle energy calculations using the spectral decomposition of the static dielectric matrix and we have systematically investigated its performance for a series of molecules and extended systems. The approach presented here offers several advantages: i) it does not require explicit summations over unoccupied states; ii) the dielectric matrix is represented by a small number of dielectric eigenvectors, and the storage and inversion of large dielectric matrices are avoided; iii) the use of plasmon-pole models is not necessary; iv) numerical accuracy is controlled by a single parameter, i.e., the number of dielectric eigenvalues and eigenvectors in the spectral decomposition of the dielectric matrix. These advantages allowed us to carry out GW calculations for systems with several hundreds of valence electrons, and to converge quasiparticle energies in a systematic way.

For all molecules and semiconductors (amorphous and crystalline) considered in this work, the computed quasiparticle energies show good agreement with experiments. We note that although all results presented here are for systems with less than 300 valence electrons, applications of our $G^\circ W^\circ$ approach to large systems with several hundred atoms and thousand of valence electrons are straightforward[14] and underway.[33]

TABLE IX. Calculated quasiparticle energies at points of high-symmetry for AlAs (in eV), together with available theoretical and experimental results (as quoted in Ref. 51). Energies are measured relative to the valence band maximum. Notations are the same as in Table VIII.

	Present	Ref. 51	Ref. 54	Expt.
Γ_{1v}	-11.66	-11.51		
Γ'_{15v}	0.0	0.0	0.0	
Γ_{1c}	2.96	2.74	2.72	3.13
Γ_{15c}	5.07	5.06		
X_{1v}	-9.77	-9.67		
X_{2v}	-5.37	-5.55		
X_{5v}	-2.20	-2.27		-2.41
X_{1c}	2.13	2.16	1.57	2.23
X_{3c}	3.08	3.04		
L_{1v}	-10.27	-10.19		
L_{1v}	-5.82	-5.69		
L_{3v}	-0.90	-0.87		
L_{1c}	3.02	2.84	2.99	2.36
L_{1c}	5.63	5.52		
Comment		PPM	PAW	

TABLE X. Calculated quasiparticle energies at points of high-symmetry for SiC (in eV), together with available theoretical and experimental results (as quoted in Ref. 51). Energies are measured relative to the valence band maximum. Notations are the same as in Table VIII.

	Present	Ref. 51	Ref. 54	Expt.
Γ_{1v}	-15.54	-16.08		
Γ'_{15v}	0.0	0.0	0.0	
Γ_{1c}	7.26	7.19	7.23	7.4
Γ_{15c}	8.10	8.18		7.75
X_{1v}	-10.46	-10.96		
X_{3v}	-8.17	-8.44		
X_{5v}	-3.47	-3.53		
X_{1c}	2.31	2.19	1.80	2.39, 2.42
X_{3c}	5.41	5.23		5.2
L_{1v}	-12.06	-12.46		
L_{1v}	-8.92	-9.19		
L_{3v}	-1.10	-1.21		-1.15
L_{1c}	6.43	6.30	6.45	6.35
L_{3c}	8.32	8.25		8.55
Comment		PPM	PAW	

ACKNOWLEDGMENTS

This work was supported by DOE BES no. DE-FG02-06ER46262 and computer time was provided by NERSC. Part of this work was performed under the auspices of the U.S. Department of Energy at Lawrence Livermore National Laboratory under Contract DE-AC52-07A27344. T.A.P. acknowledges support from the Lawrence Scholar Program. H.-V.N. acknowledges support by the Vietnam's National Foundation for Science and Technology Development (NAFOSTED) Grant No. 103.02-2010.33.

Appendix A: Iterative calculation of dielectric eigenpotentials

In this Appendix, we present the details of our approach for the calculation of dielectric eigenvalues and eigenpotentials without computing any empty states. This is done by combining iterative diagonalization algorithms with the well-established density-functional perturbation theory technique for the calculation of charge density response to a given external perturbation.[23,24]

We first note that standard iterative diagonalization algorithms, such as conjugate-gradient, Davidson, or orthogonal iteration (with Ritz acceleration), do not require an explicit representation of the matrix to be diagonalized; instead only the result of the action of the matrix on a generic set of trial vectors is required. In the linear regime, the action of the RPA dielectric matrix ϵ on a trial potential ΔV can be written as:

$$\epsilon \Delta V = (1 - v_c \cdot \chi^\circ)\Delta V, \tag{A1}$$

and therefore, the practical problem of computing the action of ϵ on a trial potential ΔV is basically equivalent to the problem of applying χ° on ΔV. By definition the product of χ° and ΔV gives the charge density response Δn of the system to the application of the trial potential ΔV. The charge density response is obtained within first-order perturbation theory:

$$\Delta n(\mathbf{r}) = 4\ \mathrm{Re} \sum_v \psi_v^*(\mathbf{r}) \Delta\psi_v(\mathbf{r}), \tag{A2}$$

where $\Delta\psi_v(\mathbf{r})$ is the first-order variation of the KS orbital $\psi_v(\mathbf{r})$. To avoid the computation of empty states in the calculation of the charge density response, we employ the DFPT technique to determine $\Delta\psi_v(\mathbf{r})$ from the solution of a linear equation:[58]

$$[\hat{H}^\circ + \alpha \widehat{\mathrm{P}}_v - (\varepsilon_v + i\omega)]|\Delta\psi_v\rangle = -(1 - \widehat{\mathrm{P}}_v)\Delta V|\psi_v\rangle, \tag{A3}$$

where $\hat{H}^\circ$ is the unperturbed KS Hamiltonian and $\widehat{\mathrm{P}}_v = \sum_v |\psi_v\rangle\langle\psi_v|$ is the projector onto the occupied (valence) manifold. The value of the positive constant α is chosen to be larger than the valence bandwidth so that the linear equation is not singular when $i\omega \to 0$. Details of the solution of Eq. (A3) within a plane-wave pseudopotential

approach for extended systems are discussed throughly in Ref. 58.

Since the full dielectric matrix is non-Hermitian, for practical purposes it is useful to define the symmetric form $\tilde{\epsilon} = v_c^{-\frac{1}{2}} \cdot \epsilon \cdot v_c^{\frac{1}{2}}$. This form can be diagonalized by standard iterative algorithms for Hermitian problems and, if necessary, the final non-Hermitian form can be obtained by a simple similarity transformation.

Appendix B: Lanczos algorithm for computing quasiparticle corrections

As shown in Eq. 10, the evaluation of *GW* quasiparticle corrections require the evaluation of several diagonal and off-diagonal elements of the resolvent of the Hamiltonian $\widehat{\mathrm{H}}^{\circ}$ for imaginary frequencies $i\omega$. The general mathematical problem that needs to be solved can be written as:

$$g(i\omega) = \langle u|(\widehat{\mathrm{H}}^{\circ} - i\omega)^{-1}|v\rangle, \tag{B1}$$

where $\widehat{\mathrm{H}}^{\circ}$ is a generic Hermitian operator and u and v are generic vectors. The calculation of $g(i\omega)$ can be obtained by using standard iterative techniques to solve Hermitian linear systems (e.g. the conjugate gradient algorithm).[59] In this case the linear systems $(H - i\omega)|z\rangle = |v\rangle$ is solved and $g(i\omega)$ is computed as $\langle u|z\rangle$. The disadvantage of this approach is that a different linear system has to be solved for each different value of $i\omega$.

The Lanczos algorithm is known to be an efficient method to compute the resolvent of Hermitian operators by performing a single iterative recursion independent of ω.[60] The standard Lanczos algorithm is limited to the case $u = v$, however for the purpose of this work it is necessary to compute also the off-diagonal elements of $g(i\omega)$. For this task we use the Lanczos algorithm proposed in Ref. 26 and applied for the first time to *GW* calculations in Ref. 15. This algorithm generates iteratively a series of vectors $\{q_1, q_2, ...\}$ by using the following procedure:[59]

$$\begin{aligned} &q_0 = 0 \\ &q_1 = v/\sqrt{\langle v|v\rangle} \\ &\beta_{n+1}|q_{n+1}\rangle = \widehat{\mathrm{H}}^{\circ}|q_n\rangle - \alpha_n|q_n\rangle - \beta_n|q_{n-1}\rangle, \end{aligned} \tag{B2}$$

where β_{n+1} is determined in order to impose the normalisation condition $\langle q_{n+1}|q_{n+1}\rangle = 1$ and $\alpha_n = \langle q_n|\widehat{\mathrm{H}}^{\circ}|q_n\rangle$. In the orthonormal basis set of the vectors $\{q_1, q_2, ...\}$ the matrix $\widehat{\mathrm{H}}^{\circ}$ has tridiagonal form:

$$T^j = \begin{pmatrix} \alpha_1 & \beta_2 & 0 & \cdots & 0 \\ \beta_2 & \alpha_2 & \beta_3 & 0 & \vdots \\ 0 & \beta_3 & \alpha_3 & \ddots & 0 \\ \vdots & 0 & \ddots & \ddots & \beta_j \\ 0 & \cdots & 0 & \beta_j & \alpha_j \end{pmatrix}, \tag{B3}$$

where α and β are the coefficients of the Lanczos recursion (Eq. B2) and j is the maximum number of performed Lanczos iterations performed. Similar to Ref. 26 the value of $g(\omega)$ can be approximated as:

$$g(i\omega) \approx \langle \zeta^j|(T^j - i\omega)^{-1}|e_1^j\rangle, \tag{B4}$$

where ζ^{jT} is a j-dimensional vector defined as $(\langle u|q_1\rangle, \langle u|q_2\rangle), \ldots, \langle u|q_j\rangle)$ and e_1^{jT} is the j-dimensional unit vector $(1, 0, \ldots, 0)$. In general the dimension j (the number of Lanczos iterations) of the matrix T^j necessary to obtain an accurate approximation of $g(i\omega)$ is much smaller than the dimension of the full matrix $\widehat{\mathrm{H}}^{\circ}$. There are two important advantages in using Eq. B4. First, the matrix T^j and the corresponding Lanczos iterative recursion do not depend on $i\omega$. Once T^j is generated, the value of $g(i\omega)$ can be computed for many values of $i\omega$ by simple linear algebra operations in a small j-dimensional space (Eq. B4). Second, the Lanczos recursion (Eq. B2) depends only on the right vector $|v\rangle$ and different ζ^j vectors can be generated "on the fly" during the Lanczos chain in order to compute matrix elements of $g(i\omega)$ for different left vectors $\langle u|$. This feature is particularly convenient to evaluate Eq. 10, where the calculation of several off-diagonal elements ($u \neq v$) is required.

* atupham@ucdavis.edu
† nhviet@iop.vast.ac.vn
‡ Current address: CRM^2, Institut Jean Barriol, Université de Lorraine and CNRS, 54506 Vandoeuvre-lès-Nancy, France

[1] W. Kohn and L. J. Sham, Phys. Rev. **140**, A1133 (1965).
[2] M. R. Martin, *Electronic Structure: Basic Theory and Practical Methods* (Cambridge University Press, Cambridge, 2004).
[3] Y. Ping, D. Rocca, and G. Galli, Chem. Soc. Rev. **42**, 2437 (2013).
[4] G. Onida, L. Reining, and A. Rubio, Rev. Mod. Phys. **74**, 601 (2002).
[5] L. Hedin, Phys. Rev. **139**, A796 (1965).
[6] M. S. Hybertsen and S. G. Louie, Phys. Rev. B **34**, 5390 (1986).
[7] M. Jain, J. R. Chelikowsky, and S. G. Louie, Phys. Rev. Lett. **107**, 216806 (2011).
[8] R. Shaltaf, G.-M. Rignanese, X. Gonze, F. Giustino, and A. Pasquarello, Phys. Rev. Lett. **100**, 186401 (2008).
[9] K. S. Thygesen and A. Rubio, Phys. Rev. B **77**, 115333 (2008).

[10] P. Umari, G. Stenuit, and S. Baroni, Phys. Rev. B **79**, 201104 (2009).
[11] B.-C. Shih, Y. Xue, P. Zhang, M. L. Cohen, and S. G. Louie, Phys. Rev. Lett. **105**, 146401 (2010).
[12] G. Samsonidze, M. Jain, J. Deslippe, M. L. Cohen, and S. G. Louie, Phys. Rev. Lett. **107**, 186404 (2011).
[13] I. Tamblyn, P. Darancet, S. Y. Quek, S. A. Bonev, and J. B. Neaton, Phys. Rev. B **84**, 201402 (2011).
[14] H.-V. Nguyen, T. A. Pham, D. Rocca, and G. Galli, Phys. Rev. B **85**, 081101 (2012).
[15] P. Umari, G. Stenuit, and S. Baroni, Phys. Rev. B **81**, 115104 (2010).
[16] F. Giustino, M. L. Cohen, and S. G. Louie, Phys. Rev. B **81**, 115105 (2010).
[17] J. A. Berger, L. Reining, and F. Sottile, Phys. Rev. B **82**, 041103 (2010).
[18] C. Friedrich, M. C. Müller, and S. Blügel, Phys. Rev. B **83**, 081101 (2011).
[19] W. von der Linden and P. Horsch, Phys. Rev. B **37**, 8351 (1988).
[20] R. W. Godby and R. J. Needs, Phys. Rev. Lett. **62**, 1169 (1989).
[21] G. E. Engel and B. Farid, Phys. Rev. B **47**, 15931 (1993).
[22] M. Stankovski, G. Antonius, D. Waroquiers, A. Miglio, H. Dixit, K. Sankaran, M. Giantomassi, X. Gonze, M. Côté, and G.-M. Rignanese, Phys. Rev. B **84**, 241201 (2011).
[23] H.-V. Nguyen and S. de Gironcoli, Phys. Rev. B **79**, 205114 (2009); F. Gygi and A. Baldereschi, *ibid.* **34**, 4405 (1986).
[24] D. Lu, F. Gygi, and G. Galli, Phys. Rev. Lett. **100**, 147601 (2008); H. F. Wilson, D. Lu, F. Gygi, and G. Galli, Phys. Rev. B **79**, 245106 (2009); H. F. Wilson, F. Gygi, and G. Galli, *ibid.* **78**, 113303 (2008).
[25] A. Baldereschi and E. Tosatti, Solid State Comm. **29**, 131 (1979); R. Car, E. Tosatti, S. Baroni, and S. Leelaprute, Phys. Rev. B **24**, 985 (1981); M. S. Hybertsen and S. G. Louie, *ibid.* **35**, 5585 (1987).
[26] D. Rocca, R. Gebauer, Y. Saad, and S. Baroni, J. Chem. Phys. **128**, 154105 (2008).
[27] H. N. Rojas, R. W. Godby, and R. J. Needs, Phys. Rev. Lett. **74**, 1827 (1995).
[28] M. M. Rieger, L. Steinbeck, I. White, H. Rojas, and R. Godby, Computer Physics Communications **117**, 211 (1999).
[29] P. Giannozzi, S. Baroni, N. Bonini, M. Calandra, R. Car, C. Cavazzoni, D. Ceresoli, G. L. Chiarotti, M. Cococcioni, I. Dabo, A. D. Corso, S. de Gironcoli, S. Fabris, G. Fratesi, R. Gebauer, U. Gerstmann, C. Gougoussis, A. Kokalj, M. Lazzeri, L. Martin-Samos, N. Marzari, F. Mauri, R. Mazzarello, S. Paolini, A. Pasquarello, L. Paulatto, C. Sbraccia, S. Scandolo, G. Sclauzero, A. P. Seitsonen, A. Smogunov, P. Umari, and R. M. Wentzcovitch, J. Phys.: Condens. Matt. **39**, 395502 (2009).
[30] H.-V. Nguyen and G. Galli, J. Chem. Phys. **132**, 044109 (2010).
[31] Y. Li, D. Lu, H.-V. Nguyen, and G. Galli, J. Phys. Chem. A **114**, 1944 (2010).
[32] (), a cubic cell of 30 a.u. with periodic boundary conditions and a plane-wave basis set with an energy cutoff of 40 Ry were used to simulate the benzene molecule. Norm-conserving pseudopotentials H.pz-vbc.UPF and C.pz-vbc.UPF were taken from the quantum espresso distribution.
[33] C. Zhang, T. Anh Pham, F. Gygi and G. Galli (preprint).
[34] J. P. Perdew, K. Burke, and M. Ernzerhof, Phys. Rev. Lett. **77**, 3865 (1996).
[35] National Institute of Standard, NIST Chemistry webbook, http://webbook.nist.gov/chemistry/.
[36] X. Blase, C. Attaccalite, and V. Olevano, Phys. Rev. B **83**, 115103 (2011).
[37] M. J. van Setten, F. Weigend, and F. Evers, Journal of Chemical Theory and Computation **9**, 232 (2013).
[38] (), we note that the ground state calculations of Ref. 36 were performed starting from a double-ζ+polarization (DZP) basis; then the numerical radial part was fitted by up to five contracted Gaussians in order to exploit the computational efficiency of Gaussian basis sets to facilitate *GW* calculations.
[39] L. A. Curtiss, K. Raghavachari, P. C. Redfern, and J. A. Pople, The Journal of Chemical Physics **106**, 1063 (1997).
[40] X. Gonze, B. Amadon, P.-M. Anglade, J.-M. Beuken, F. Bottin, P. Boulanger, F. Bruneval, D. Caliste, R. Caracas, M. Ct, T. Deutsch, L. Genovese, P. Ghosez, M. Giantomassi, S. Goedecker, D. Hamann, P. Hermet, F. Jollet, G. Jomard, S. Leroux, M. Mancini, S. Mazevet, M. Oliveira, G. Onida, Y. Pouillon, T. Rangel, G.-M. Rignanese, D. Sangalli, R. Shaltaf, M. Torrent, M. Verstraete, G. Zerah, and J. Zwanziger, Computer Physics Communications **180**, 2582 (2009).
[41] J. P. Perdew, M. Ernzerhof, and K. Burke, The Journal of Chemical Physics **105**, 9982 (1996); C. Adamo and V. Barone, *ibid.* **110**, 6158 (1999).
[42] J. Heyd, G. E. Scuseria, and M. Ernzerhof, The Journal of Chemical Physics **118**, 8207 (2003).
[43] J. P. Perdew and A. Zunger, Phys. Rev. B **23**, 5048 (1981).
[44] C. Rostgaard, K. W. Jacobsen, and K. S. Thygesen, Phys. Rev. B **81**, 085103 (2010).
[45] F. Bruneval and M. A. L. Marques, Journal of Chemical Theory and Computation **9**, 324 (2013).
[46] M. K. Y. Chan and G. Ceder, Phys. Rev. Lett. **105**, 196403 (2010).
[47] X. Ren, P. Rinke, V. Blum, J. Wieferink, A. Tkatchenko, A. Sanfilippo, K. Reuter, and M. Scheffler, New Journal of Physics **14**, 053020 (2012).
[48] S. Baroni and R. Resta, Phys. Rev. B **33**, 7017 (1986).
[49] A. Baldereschi and E. Tosatti, Phys. Rev. B **17**, 4710 (1978).
[50] A. Fleszar and W. Hanke, Phys. Rev. B **56**, 10228 (1997).
[51] W. G. Aulbur, M. Städele, and A. Görling, Phys. Rev. B **62**, 7121 (2000).
[52] M. Rohlfing, P. Krüger, and J. Pollmann, Phys. Rev. B **48**, 17791 (1993).
[53] Y. Li and G. Galli, Phys. Rev. B **82**, 045321 (2010).
[54] S. Lebègue, B. Arnaud, M. Alouani, and P. E. Bloechl, Phys. Rev. B **67**, 155208 (2003).
[55] T. A. Pham, T. Li, S. Shankar, F. Gygi, and G. Galli, Phys. Rev. B **84**, 045308 (2011).
[56] T. A. Pham, T. Li, S. Shankar, F. Gygi, and G. Galli, Applied Physics Letters **96**, 062902 (2010).
[57] J. Bauer, physica status solidi (a) **39**, 411 (1977).
[58] S. Baroni, S. de Gironcoli, A. D. Corso, and P. Giannozzi, Rev. Mod. Phys. **73**, 515 (2001).
[59] Y. Saad, *Iterative Methods for Sparse Linear Systems*, 2nd ed. (SIAM, Philadelphia, 2003).
[60] D. W. Bullet, R. Haydock, V. Heine, and M. Kelly (Academic Press, New York, 1980).